DMD Fast Forward. Published on February 20, 2019 as DOI: 10.1124/dmd.118.085811
This article has not been copyedited and formatted. The final version may differ from this version.

Oxidative Deamination of Emixustat by Human Vascular Adhesion Protein-1/Semicarbazide-sensitive Amine Oxidase

Michael J Reid, Russell Eyre, and Terry Podoll

Acucela Inc., Seattle, WA (MJR)

MavuPharma, Kirkland, WA (RE)

IV-PO, LLC, Seattle, WA (TP)

a) Emixustat oxidative deamination by human VAP-1 (SSAO).

b) Michael Reid, PhD, 818 Stewart Street, Seattle, WA, 98101, 425-308-1456, mjr33_33@yahoo.com.

c) Number of text pages: 27

Number of tables: 4

Number of figures: 7

Number of references: 44

Number of words in the Abstract: 221

Number of words in the Introduction: 718

Number of words in the Discussion: 1737

d) List of nonstandard abbreviations (alphabetical order): AMD = age-related macular degeneration, AOC = amine oxidase copper-containing, A2E = N-retinylidene-N-retinylethanolamine, BA = benzylamine, BAL = benzaldehyde, BALDNP = benzaldehyde dinitrophenylhydrazone, CPQ = carboxyprimaquine, DEABAL = 4-diethylamino-benzaldehyde, DNPH = 2,4-dinitrophenylhydrazine, hAM = human aorta membranes, hLM = human liver microsomes, hP = human plasma, hUCM = human umbilical cord membranes, LOX = lysyl oxidase, MPA = mobile phase A, PQ = primaquine, pTALDNP = *p*-tolualdehyde dinitrophenylhydrazone, RPE65 = retinal pigmented epithelium protein 65, SSAO = semicarbazide-sensitive amine oxidase, VAP-1 = vascular adhesion protein-1

Abstract

Emixustat potently inhibits the visual cycle isomerase RPE65 to reduce the accumulation of toxic bisretinoid by-products that lead to various retinopathies. Orally administered emixustat is cleared rapidly from the plasma, with little excreted unchanged. The hydroxypropylamine moeity that is critical in emixustat's inhibition of RPE65 is oxidatively deaminated to three major carboxylic acid metabolites that appear rapidly in plasma. These metabolites greatly exceed the plasma concentrations of emixustat and demonstrate formation-rate limited metabolite kinetics. This study investigated in vitro deamination of emixustat in human vascular membrane fractions, plasma and recombinant human vascular adhesion protein-1 (VAP-1); demonstrating single enzyme kinetics for the formation of a stable aldehyde intermediate (ACU-5201) in all in vitro systems. The in vitro systems employed herein established sequential formation of the major metabolites with addition of assay components for aldehyde dehydrogenase (ALDH) and cytochrome P450 (CYP). Reaction phenotyping experiments using selective chemical inhibitors and recombinant enzymes of monoamine oxidase (MAO), VAP-1 and lysyl oxidase (LOX), showed that only VAP-1 deaminated emixustat. In individually-derived human vascular membranes from umbilical cord and aorta, rates of emixustat deamination were highly correlated to VAP-1 marker substrate activity (benzylamine) and VAP-1 levels measured by ELISA. In donor-matched plasma samples, soluble VAP-1 activity and levels were lower than in aorta membranes. A variety of potential co-medications did not strongly inhibit emixustat deamination in vitro.

Introduction

Emixustat (CAS number 1141777-14-1, ACU-4429) is a potent orally administered small-molecule inhibitor of retinal pigment epithelium 65 (RPE65) under clinical development by Acucela Inc. for the potential treatment of various retinopathies including Stargardt disease and proliferative diabetic retinopathy. RPE65 is a key isomerohydrolase enzyme in the pathway that regenerates the visual chromophore (11-cis retinal) in vertebrate retinal tissue. Emixustat decreases the levels of vitamin A derivatives (11-cis- and all-trans-retinal) and the accumulation of toxic lipid-retinoid by-products (e.g. A2E and lipofuscin) that result in dysfunction and eventual death of the specialized photoreceptor-containing cells of the retina (Bavik et al., 2015). While important advances have been achieved in treatment of the wet form of age-related macular degeneration (AMD; Gower et al., 2016) using injectable vascular endothelial growth factor inhibitors, oral administration for retinal diseases remains an attractive objective given the infection risks and frequent office visits associated with intravitreal injection (Awh, 2016).

Emixustat was designed to treat the retina following oral administration by focusing on potent and durable pharmacologic activity against RPE65 while displaying rapid systemic elimination. Preclinical demonstration of these traits translated well to clinical application in a Phase 1 study wherein dose-dependent effects were measured in the retina more than 24 hours after dose, at a time when emixustat levels were very low due to its rapid elimination (4 – 6 hour half-life in plasma; Kubota et al., 2012). Emixustat absorption was also rapid with T_{max} values ranging from 3 – 5 hours while no accumulation was observed upon repeated-dose administration (Kubota et al., 2014). A human ADME study characterized three major (ie, ≥10% of total systemic ^{14}C exposure) circulating metabolites, ACU-5116, ACU 5124, and ACU-5149, accounting for 11.5%, 29.0%, and 10.6% of the total area under the plasma drug concentration-time curve

(AUC) of circulating radioactivity (Fitzsimmons et al., 2018). In this study >90% emixustat dose-related radioactive material was excreted via the urine as metabolites, similar to nonclinical species (data on file).

Preclinical in vivo metabolism of emixustat was very similar across rat, dog, and monkey (Podoll et al., 2013). The three major metabolites are carboxylic acids that are products of oxidative deamination of the primary amine of emixustat (Fitzsimmons et al., 2018). Two of the three metabolites, ACU-5124 and ACU-5149, were secondary metabolites that had also been differentially hydroxylated in the cyclohexyl ring. In human hepatocytes, primary hydroxylation to the cyclohexanols dominated the product formation observed; averaging 26% of radioactivity, and only 4 – 9% observed as the oxidatively deaminated carboxylic acids (Fitzsimmons et al., 2018). In human liver microsomes no oxidative deamination was observed and NADPH-dependent turnover of [^{14}C]emixustat was low, yet CYP2D6 and CYP3A4 were identified as capable of catalyzing the hydroxylation of emixustat in vitro when using the cDNA-expressed CYP isoforms (data on file). Other extra-hepatic, human in vitro systems were then used to characterize the predominant oxidative deamination reaction observed in the human ADME clinical trial.

Initial studies focused on monoamine oxidases (MAO), yet emixustat was not a substrate for MAO (data on file), so alternative methods were sought to characterize its oxidative deamination. The first evidence of vascular adhesion protein-1/semicarbazide-sensitive amine oxidase (VAP-1/SSAO from here forward referred to as VAP-1) involvement in the metabolism of emixustat was revealed during cross-species plasma protein binding study (Fitzsimmons et al., 2018; with additional nonclinical species data on file). Plasma stability assessments demonstrated inter-species differences that were consistent with the highest soluble plasma deamination activity observed in pig and dog (Schwelberger 2007). Prior studies have used human umbilical artery microsomes

(hUCM) to demonstrate the involvement of VAP-1 in the metabolism of tresperimus (Claud et al., 2002). Since then potent, selective VAP-1 inhibitors have been developed (Salter-Cid et al., 2005) and recombinant VAP-1 has become commercially available. The results of human in vitro reaction phenotyping for the oxidative deamination of emixustat are described here. Since emixustat was targeting retinopathies that are more prevalent in adults aged 65 years and above (e.g. AMD) and this population can have inflammatory diseases impacting VAP-1 (Salmi et. al., 1993; Pannekoek et al., 2015), human aorta tissue was obtained from elderly donors to characterize emixustat oxidative deamination in this patient population. Once established, the in vitro model was used to assess the impact of potential VAP-1 inhibitors on emixustat and the impact of emixustat on the VAP-1 catalyzed oxidative deamination of model substrate, benzylamine (BA).

Materials and Methods

Materials. Emixustat hydrochloride (99.7% chemical purity) was manufactured by IRIX Pharmaceuticals (Florence, SC). ACU-4861 [(1R,4r)-4-((3-((R)-3-amino-1-hydroxypropyl)phenoxy)methyl)cyclohexan-1-ol], ACU-5116 [(R)-3-(3-(cyclohexylmethoxy)phenyl)-3-hydroxypropanoic acid], ACU-5124 [(R)-3-hydroxy-3-(3-(((1r,4R)-4-hydroxycyclohexyl)methoxy)phenyl)propanoic acid], ACU-5141 (d11-ACU-5116), ACU-5142 (d3-ACU-5124) and ACU-5201 [(E)-3-(3-(cyclohexylmethoxy)phenyl)acrylaldehyde] were prepared by Acucela (Bothell, WA) as described previously (Fitzsimmons et al., 2018, supplemental). LJP-1207 [N′-(2-phenyl-allyl)-hydrazine hydrochloride] was also prepared and characterised by Acucela according to previously published methods (Salter-Cid et al., 2005). Acetic acid, methanol (HPLC grade), phosphate buffered saline, sodium bicarbonate and water (HPLC grade) were obtained from Fisher Scientific USA (Pittsburg, PA). All other chemicals and reagents were obtained from Sigma-Aldrich (St. Louis, MO).

Recombinant human VAP-1, the ELISA kit for human VAP-1, anti-human VAP-1 antibody as well as recombinant human Lysyl Oxidase Homolog 2 (LOXL2) were obtained from R&D Systems (Minneapolis, MN). Anti-mouse HRP antibody was obtained from Promega (Madison, WI). Human liver microsomes (hLM; UltraPool™ HLM 150 Mixed Gender; lot # 38290) were obtained from BD Biosciences (Woburn, MA). Human umbilical cord membranes (hUCM), and elderly human aorta membranes (hAM) with matching heparinized plasma samples from the elderly humans were prepared under contract by BioIVT (Baltimore, MD). Twenty individual lots each of hUCM, and hAM and 18 donor-matched (to hAM) individual plasma samples were provided to assess inter-individual variability of VAP-1 activity. An 8-donor pool of hUCM and a 20-donor pool of hAM were also provided to determine the kinetics of VAP-1 activity. Aorta tissues were obtained from individuals that were at least 65 years

of age with the following demographics:11 male (M) and 9 female (F), 3 African-America, 4 non-white Hispanic and 13 Caucasian with body mass index ranging from 16.9 to 43. Eight individuals were identified as having diabetes and 17 had cardiovascular complications and/or hypertension.

Sequential Oxidative Metabolism of Emixustat in Human Tissue. Pooled hUCM, NAD+, emixustat and its hydroxycyclohexyl metabolite (ACU-4861) were prepared in 10 mM sodium bicarbonate buffer, pH 7.4, and kept on wet ice until added to incubations. Final incubation volumes of hUCM reactions were 0.2 ml at a final protein concentration 0.1 mg/ml with final concentrations of substrates (100 μM emixustat or ACU-4861), and the cofactor NAD^+ (1 mM). Reactions were started by the addition of hUCM immediately followed by the addition of NAD^+ and stopped after 20 minutes with the addition of 0.2 ml of acetonitrile (ACN), vortexed briefly and centrifuged at 13,000 x g for 10 minutes to precipitate proteins. Supernatants were filtered through 0.2 μm polypropylene filter membranes (Captiva, Agilent) and loaded onto 96-well plates.

Human liver microsomes (hLM), NADPH, and the deaminated carboxylic acid metabolite (ACU-5116) were prepared in 10 mM potassium phosphate buffer, pH 7.4, and kept on wet ice until added to incubations. Final incubation volumes of hLM reactions were 0.2 ml, final microsomal protein concentrations were 1.0 mg/ml, final ACU-5116 concentrations were 100 μM and final concentrations of NADPH were 1 mM. Reactions were started by the addition of NADPH to hLM incubations preincubated at 37°C for 3 minutes. Reactions were stopped after 20 minutes with the addition of 0.1 ml of ACN, vortexed briefly and centrifuged at 13,000 x *g* for 10 minutes to precipitate proteins. Supernatants were filtered through 0.2 μm polypropylene filter membranes (Captiva, Agilent) and loaded onto 96-well plates.

In Vitro Metabolism of Emixustat in Human Sources of VAP-1. In vitro metabolism of emixustat by human sources of VAP-1 was determined by measuring the amount of its

stable aldehyde product (ACU-5201) formed per minute per mg protein (or ml plasma) in triplicate. Final incubation volumes were 0.1 ml and the amount of VAP-1 source and incubation time were linearly optimized. Pooled and individual lots of hUCM or hAM were prepared at a final protein concentration 0.1 mg/ml and recombinant human VAP-1 was prepared at a final protein concentration 0.01 mg/ml while human plasma (hP) was assayed volumetrically (0.05 ml) in 10 mM sodium bicarbonate buffer, pH 7.4 ($NaHCO_3$ buffer). Stock solutions of emixustat and inhibitors were also prepared in $NaHCO_3$ buffer and were pre-incubated at 37°C together (when inhibition was tested) prior to adding the enzyme source. Human sources of VAP-1 were kept on dry ice until thawed at 37°C prior to diluting with $NaHCO_3$ buffer. When possible, timed incubations (10 minutes for hUCM, hAM and rhVAP-1 and 30 minutes for plasma) were started immediately by the addition of the enzyme source and stopped by the addition of 0.2 ml of ACN fortified with 10 ng/ml of 4-diethylamino-benzaldehyde (DEABAL as an internal standard), vortexed briefly and centrifuged at 13,000 x *g* for 10 minutes to precipitate proteins. During simultaneous incubations of tissue from several individuals the membrane preparations were kept on wet ice until aliquoted and brought to 37°C before combination with substrate. Emixustat concentrations ranged from 5.0 – 500 µM when determining enzyme kinetic parameters in the various human sources of VAP-1 and between 60-160 µM when assessing interindividual activity and inhibition. Supernatants were filtered through 0.2 µm PVDF membranes (Captiva, Agilent) and loaded onto 96-well plates for quantification by LC-MS/MS.

LC-MS/MS Quantitation of Emixustat's Primary In Vitro Aldehyde Metabolite (ACU-5201). Although ACU-5201 has only been observed in vitro (Fitzsimmons et al., 2018), the proposed intermediate aldol (Figure 1) has not been identified nor could it be synthesized due to apparent instability during isolation and purification. The amount of ACU-5201 formed in VAP-1 incubations was quantitated by LC-MS/MS. ACU-5201

standard was diluted in ACN and used for preparation of calibration standard stock solutions that were added at 10% (v:v) to appropriate volumes of incubation reaction media and acetonitrile to match the sample incubations.

Liquid chromatography (LC20AD; Shimadzu, Pleasanton, CA) separation was achieved on a Poroshell 120 Phenyl Hexyl, 2.1 x 50 mm, 2.7 µm column (Agilent) using a step gradient of 10 mM ammonium formate (mobile phase A: MPA) and ACN at 0.45 ml/min as follows: 0.25 min 60% MPA, 0.25 min linear gradient to 17% MPA, 0.75 min 17% MPA, 0.25 min linear gradient to 8% MPA, then 0.5 min at 8% MPA before flushing with 100% ACN and re-equilibrating to 60% MPA. Column temperature was set to 30°C while autosampler temperature was set to 10°C. Samples (20 µl) were injected with an external rinse program using 100% ACN.

The mass spectrometer (API5000; SCIEX, Redwood City, CA) was operated in the positive ion mode and MRM scan type. The first and third quadrupoles were set to detect the positively charged molecular ions $[M+H]^+$ and fragments of ACU-5201 (m/z 245.2→103.1 Da) and DEABAL (m/z 178.2→106.1 Da) with unit resolution in both quadrupoles. Compound-dependent MS/MS parameters for quantitating ACU-5201 and DEABAL were: Declustering Potential = 60.0 and 175.0 V; Entrance Potential = 10.0 V; Collision Energy = 37.0 and 40.0 V; Exit Potential = 15.0 and 17.0 V, respectively. Source and gas parameters were: Collision Gas = 8 psi, Curtain Gas = 11 psi, Nebulizer Gas = 50 psi, Turbo Gas = 60 psi, ESI Voltage = 5500 V and Temperature = 675°C.

In Vitro Deamination of Benzylamine in Human Sources of VAP-1. Oxidative deamination of benzylamine (BA) was employed as a biomarker of VAP-1/SSAO enzymatic activity in human sources of VAP-1 in vitro. The rate of BA deamination was determined by measuring the amount of benzaldehyde (BAL) formed per minute per mg protein (or ml plasma) in triplicate (only duplicates for some plasma incubations). Final incubation volumes were 0.1 ml and the amount of VAP-1 source and incubation time

were linearly optimized. Pooled and individual lots of hUCM or hAM were prepared at a final protein concentration 0.1 mg/ml and recombinant human (rh) VAP-1 was prepared at a final protein concentration 0.0025 mg/ml while plasma was assayed volumetrically (0.05 ml) in $NaHCO_3$ buffer. Final reaction volumes were 0.1 ml and timed incubations were started by the addition of the enzyme source at 37°C. When inhibition and interindividual activity was tested, BA concentrations were 80 µM for membrane and recombinant sources and 200 µM for plasma. Reactions were stopped after 10 minutes for membrane and recombinant sources and after 30 minutes for plasma by the addition of 0.2 ml of 60/40 ACN/MeOH fortified with 5 µM of the internal standard *p*-tolualdehyde dinitrophenylhydrazone (pTALDNP), vortexed briefly and centrifuged at 13,000 x *g* for 10 minutes to precipitate proteins. Supernatants (0.25 ml) were filtered through 0.2 µm PVDF membranes (Captiva, Agilent) and loaded onto 96-well plates with each well containing 50 µl of 2,4-dinitrophenylhydrazine (DNPH; 3 mg/ml) solution. Derivatizations were incubated at 40°C for 20 minutes and stopped by the addition of 10 µl of 25% formic acid, and then vortexed briefly prior to loading into the autosampler. Initial incubations in hUCM did not incorporate the internal standard in a reaction stop solution of acetonitrile with 2% formic acid and these derivatizations were not stopped with formic acid. These method optimizations resulted in improved recovery of the benzaldehyde dinitrophenylhydrazone (BALDNP) by > 50% across the calibration range when compared to authentic BALDNP standard spiked into reaction mixtures (data not shown), affording better sensitivity to assess inhibition.

LC-MS/MS Quantitation of Derivatized Benzaldehyde. The amount of derivatized benzaldehyde (BALDNP) formed in VAP-1 incubations was quantitated by LC-MS/MS. Benzaldehyde standard was diluted in methanol to 4 mM and used for preparation of calibration standard and QC stock solutions. To match the sample incubations, stock solutions of BAL were added at 10% (v:v) to appropriate volumes of incubation reaction

media and internal standard solution. Calibration standards and QCs were derivatized along with incubation samples following centrifugation according to the procedure outlined above.

Liquid chromatography separation was achieved on a Kinetix Biphenyl 2.5 µm, 2 x 30 mm column (Phenomenex) using a step gradient of 0.15 formic acid (MPA) and 60% ACN/40% MeOH (mobile phase B) at 0.8 ml/min as follows: 0.8 min 34% MPA, 1.0 min linear gradient to 2% MPA, then 1.0 min 2% MPA before re-equilibrating to 34% MPA. Column temperature was set to 30 °C while autosampler temperature was set to 6°C. Samples (20 µl) were injected with an external rinse program using 100% ACN.

The mass spectrometer was operated in the positive ion mode and MRM scan type. The first and third quadrupoles were set to detect the positively charged molecular ions [M+H]+ and fragments of BALDNP (m/z 287.2→104.1 Da) and pTALDNP (m/z 301.1→118.3 Da) with unit resolution in both quadrupoles. Compound-dependent MS/MS parameters for quantitating BALDNP and pTALDNP were: Declustering Potential = 70.0 V, Entrance Potential = 10.0 V, Collision Energy = 24.0 V and Exit Potential = 15.0 V. Source and gas parameters were: Collision Gas = 10 psi, Curtain Gas = 14 psi, Nebulizer Gas = 50 psi, Turbo Gas = 55 psi, ESI Voltage = 5200 V and Temperature = 700°C.

Quantification of VAP-1 by ELISA. Vascular adhesion protein-1 levels in membranes and plasma were quantified using the R&D Systems Quantikine ELISA for human VAP-1. The ELISA was performed according to the instructions in the manual. The samples were diluted 1:100 with Calibrator Diluent RD6X. The optical density for the plate was read at 450 nm and 570 nm. To account for wavelength correction, the 570 nm value was subtracted from the 450 nm value. The background value (value from well without any sample, standard or control) was subtracted from all wells. VAP-1 concentrations (ng/ml) for all samples determined from the calibration standards were normalized to total protein

concentrations determined by standard methods (Smith et al., 1985) into μg VAP-1/mg total protein.

Clinical Study Analyses. Plasma concentrations of emixustat and its three major metabolites were determined in a clinical pharmacology study titled: Pharmacokinetic and Pharmacodynamic Study of Emixustat Hydrochloride in Subjects With Geographic Atrophy Associated With Dry Age-Related Macular Degeneration (Dugel et al., 2015) using a validated LC-MS/MS method (Podoll et al., 2018). The study was performed in accordance with the ethical principles stated in the Declaration of Helsinki, FDA regulation 21 CFR, Parts 50, 56, and 312, and International Conference on Harmonization guidelines for good clinical practice. The protocol, advertisement, and Informed Consent Form (ICF) were reviewed and approved by the Institutional Review Board. Written informed consent for the study was obtained from all subjects before protocol-specific procedures were carried out. Emixustat was administered orally at doses ranging from 2 to 10 mg once daily with plasma samples collected to meet study objectives.

Data Analysis. Linear regression analysis of calibration curve data and resulting unknown sample concentration determination was performed with Analyst software (versions 1.5.1 through 1.6.2; AB Sciex, Redwood City, CA) using the ratio of product to internal standard as the dependent variable. Mathematical conversion of product formation data and basic statistical calculations were performed using Microsoft Excel 2010. Michaelis-Menten and other enzyme kinetic data analysis was performed using nonlinear hyperbolic one-site binding or competition fits on GraphPad Prism software (versions 4-7; La Jolla, CA). Log values from the ELISA standards (log ng/ml VAP-1) were plotted against the corrected OD570 also using GraphPad Prism with the 4-parameter logistic curve fit. Pearson's and Spearman's rank correlation analysis and ANOVA of VAP-1 metabolic activities and VAP-1 levels was also performed using

GraphPad Prism software. Semi-log concentration-time plots for the clinical pharmacology study were also constructed using GraphPad Prism software. All noncompartmental pharmacokinetic (PK) analyses were performed using WinNonlin™ (version 6.3, Certara L.P., Princeton, NJ).

Results

Oxidative Deamination of Emixustat. The three major circulating metabolites observed following the dosing of [^{14}C]emixustat during a human ADME clinical trial, ACU-5116, ACU-5124, and ACU-5149, were all carboxylic acid products of oxidative deamination of the primary amine. While the intermediate aldehydes were not observed in vivo in human plasma, ACU-5201 was identified during in vitro human plasma stability tests using [^{14}C]emixustat (Fitzsimmons, et al., 2018). Similar to a previous tresperimus report (Claud et al., 2001), exposure of emixustat was increased approximately 2-fold in rats following prior administration of hydralazine and semicarbazide, suggesting the rate-determining role of VAP-1 in the elimination of emixustat (data on file). The metabolic scheme shown in Figure 1 was proposed to initiate in vitro studies to characterize the enzymology relevant to the human in vivo metabolism of emixustat. Range-finding incubations of emixustat in human umbilical cord membranes (hUCM), an established source of VAP-1 activity, suggested the ACU-5201 aldehyde was the predominant in vitro product. Further experiments were conducted with emixustat to confirm that ACU-5201 formation kinetic parameters could be accurately determined.

To monitor formation of the carboxylic acid metabolite, a quantitative method for ACU-5116 using synthetic reference standard and deuterium-labeled internal standard was established. Emixustat (50 µM; 80% maximal rate) was incubated at 37ºC with hUCM at 0, 0.1, and 0.25 mg/ml total protein up to 16 minutes. While levels of ACU-5116 were BLQ, ACU-5201 was formed linearly with both time and protein at concentrations ranging from approximately 100 to 1000 ng/ml. Although several oxidases may contribute to the rapid oxidation of the aldehyde intermediate in vivo, the role of aldehyde dehydrogenase (ALDH) in the conversion to the carboxylic acid was

tested. Emixustat (16 μM; at K_M, see below) was added to pooled hUCM (1 mg/ml protein) in the presence and absence of NAD^+. High levels of ACU-5116 were observed in the presence of NAD^+ and were nearly the molar equivalent to the decrease in the formation of ACU-5201 when compared to the incubations without NAD^+ (Figure 2A). Experiments exploring the formation route(s) of the secondary metabolite, ACU-5124, resulting from both oxidative deamination of the primary amine and hydroxylation of the cyclohexyl ring of emixustat (Figure 1), were conducted with two primary metabolites of emixustat. To maximize potential product formation, 100 μM ACU-5116 was incubated with human liver microsomes (1 mg/ml protein) in the presence and absence of NADPH. NADPH-dependent formation of ACU-5124 was observed, confirming that ACU-5116 is a substrate for CYP enzymes resulting in the formation of ACU-5124. ACU-4861 (100 μM), a monohydroxylated metabolite previously shown to be formed by CYP enzymes in human hepatocytes (Fitzsimmons et al., 2018) was also incubated in order to maximize product formation with pooled hUCM (1 mg/ml protein) for 20 minutes in the presence and absence of NAD^+. NAD^+-dependent formation of the carboxylic acid metabolite, ACU-5124, was observed demonstrating that its formation could also proceed from initial hydroxylation of emixustat, followed by oxidative deamination and aldehyde oxidation of the monohydroxylated amine metabolite (Figure 2B). Given these results, vascular membranes were used to generate kinetic parameters for the oxidative deamination of emixustat via ACU-5201 formation rates as an in vitro model for assessing the variability of VAP-1 reaction rates across a population of individually-derived vascular tissues and for the assessment of emixustat as a potential victim of in vitro drug interactions driven by inhibition of VAP-1.

Enzyme kinetics were assessed for emixustat deamination activity with the linearly optimized protein concentration (or volume of plasma) and incubation time for

rhVAP-1, hUCM, human aorta membranes (hAM) and human plasma (hP). Michaelis-Menten kinetic constants were determined by fitting the rate equation for a single-enzyme using nonlinear regression; substrate saturation data are presented graphically in Figure 3. Mean VAP-1 enzyme kinetic constants in rhVAP-1, and pooled hUCM, hAM, and hP are presented in Table 1. The apparent Michaelis constant (K_M) values for the formation of ACU-5201 of 13, 14.7 and 15.6 μM in rhVAP-1, hUCM and hAM, respectively, are in very close agreement indicating that the different human sources of the VAP-1 enzyme had the same binding affinity for emixustat. These data confirmed that in vitro product formation of the aldehyde metabolite was adequate to assess the oxidative deamination of emixustat. Limited turnover of emixustat was observed in hP. The reaction rates did not reach saturating conditions resulting in an overestimation of the apparent K_M in hP when compared to other VAP-1 sources.

In Vitro VAP-1 Oxidative Deamination Activity. To correlate the amine oxidase activity in human vascular membrane preparations (hUCM and hAM) and plasma with emixustat oxidative deamination rates, we adapted an assay for the commonly used amine oxidase substrate, benzylamine (BA), which yields benzaldehyde (BAL). Although BA is not a physiologic substrate for VAP-1, there are numerous assays based on the oxidative deamination of BA to form BAL as a marker substrate for quantifying various amine oxidase activities including: radiometric detection of extracted ^{14}C-BAL (Lizcano et al., 1998), HPLC with fluorometric detection of derivatized BAL (van Dijk et al., 1995), UV monitoring of BAL (Heuts et al., 2011) and measurement of the H_2O_2 produced using Amplex red (Holt et al., 1997). A common method used for the measurement of aldehydes is an acid catalyzed derivatization with DNPH followed by HPLC with ultraviolet or fluorometric detection (Claud et. al., 2002.). A direct injection LC-MS/MS method of the DNPH-derivatized BAL (BALDNP) was developed to

DMD Fast Forward. Published on February 20, 2019 as DOI: 10.1124/dmd.118.085811
This article has not been copyedited and formatted. The final version may differ from this version.

measure the amount of BAL formed per minute per mg protein in in vitro incubations. Following the initial experiments in hUCM, the LC-MS/MS method for BALDNP was modified slightly to improve the sensitivity of the assay in order to better characterize inhibition in latter experiments with hAM and hP. Efficiency and recovery of the 2,4, DNPH derivatization was improved by increasing the pH of the reaction stop solvent closer to 4.5 with 0.1 M ammonium acetate added to the organic solvent. These changes improved the recovery BALDNP from ~30-40% across the calibration range to >85% when compared to neat BALDNP spiked samples (data on file).

Enzyme kinetics were assessed for BA deamination activity with the linearly optimized protein concentration and incubation time for hUCM, hAM and hP (plasma volume). The Michaelis-Menten kinetic constants were determined by fitting the rate equation for a single-enzyme using nonlinear regression. Mean VAP-1 enzyme kinetic constants in rhVAP-1, and pooled hUCM, hAM and hP are presented in Table 2. The apparent BA K_M values for the formation of BAL of 56.6, 78.7, 78.9 and 75.2 μM, in rhVAP-1 and pooled hUCM, hAM and hP, respectively. These K_M values are similar to 63.5 ± 9.5 μM previously reported for BA deamination in human umbilical artery microsomes (Claud et al., 2002) indicating that the different human sources of the VAP-1 enzyme had the same binding affinity for this marker substrate. Although the rates of product formation in plasma are much lower than in membranes or recombinant sources, the V_{max} in pooled hP was 17.6 nmol/ml/hr which is comparable to other reported clinical values for: diabetic vs normal subjects with means of 20.6 and 14.3 nmol/ml/hr, respectively (Garpenstrand et al., 1999), and chronic liver disease vs healthy normal subjects with means of 18.8 and 10.7 nmol/ml/hr, respectively (Kurkijärvi et al., 2000).

Reaction Phenotyping of VAP-1 Oxidative Deamination.

Correlation Analysis. The interindividual variability in VAP-1 activity observed across a population of tissue donors was assessed in hUCM, hAM and hP acquired from

commercial sources. Saturating concentrations of emixustat and BA were incubated in triplicate for the individual sources of VAP-1 at the linearly optimized conditions. Mean rates of ACU-5201 formation ranged from 36.4 to 170, 5.82 to 100 and 0.748 to 7.51 pmol/min/mg protein in hUCM, hAM and hP, respectively. The 10-fold difference in emixustat deamination in hP and 17-fold difference in hAM had more variability than the 4.7-fold difference in hUCM, however the mean rate of 20 individuals in both hUCM and hAM were very similar at 44.7 and 49.4 pmol/min/mg protein, respectively. Mean rates of BAL product formation ranged from 13.7 to 40.4, 4.16 to 36.6 and 0.0637 to 1.17 nmol/min/mg protein in hUCM, hAM and hP, respectively. The 18-fold difference in BA deamination in hP and 9-fold difference in hAM also exhibited more variability than the 3-fold difference in hUCM. The interindividual variability in VAP-1 protein levels measured by ELISA was also assessed across a population of tissue donors in hUCM, hAM and hP. Mean levels of VAP-1 protein measured ranged from 267 to 1690, 168 to 506 and 0.329 to 1.10 ng/mg protein in hUCM, hAM and hP, respectively. The variability of VAP-1 measured by ELISA normalized to total protein varied less (3- to 6-fold) than the oxidative deamination activities.

Correlation constants for comparisons of individual BA deamination rates and VAP-1 protein levels to each other and to emixustat deamination activity using both Gausian (Pearson's) and nonparametric (Spearman's) analyses are presented in Table 3. Correlations of individual BA deamination rates and VAP-1 protein levels to emixustat deamination activity are graphically presented in Figure 4. VAP-1 BA deamination activity was highly correlated with the VAP-1 levels in plasma and significantly correlated in hUCM and hAM supporting the use of BA deamination as a marker for VAP-1 activity. Benzylamine deamination activity and VAP-1 protein levels were well correlated with emixustat deamination in hUCM, hAM and hP. These results indicate that interindividual variability in VAP-1 contributes to variability emixustat deamination.

Also of interest, the plasma activity or protein levels were not predictive of the oxidative deamination activity in the elderly human aorta membranes.

Recombinant Human Enzymes. Recombinant forms of human VAP-1, lysyl oxidase-like protein-2 (LOXL2; another amine oxidase copper containing), MAO-A and MAO-B (BD Gentest, Franklin Lakes, NJ) were also used to assess the specificity of this amine oxidase activity in deaminating emixustat to ACU-5201. As noted earlier, rhVAP-1 had similar affinity to emixustat as the other human tissue sources of VAP-1 with high rates of maximum reaction velocity (see Table 1 and Figure 3) affirming the deaminase activity of this enzyme for emixustat. No apparent metabolites of radiolabeled emixustat were evident after incubation with rhMAO-A and rhMAO-B for 30 minutes, while activities for the positive control substrates kynuramine and benzylamine confirmed active monoamine oxidases (data on file). In addition, no ACU-5201 was observed when incubating emixustat with rhLOXL2 for 30 minutes.

Selective Chemical Inhibitors. Selective inhibition of amine oxidase activity was also used to assess the contribution of VAP-1 and MAO-A and -B in both hUCM and hAM. Semicarbazide and LJP-1207 were co-incubated with emixustat as specific inhibitors of VAP-1, clorgyline and deprenyl were co-incubated to selectively inhibit MAO-A and MAO-B, respectively. Quinidine was tested because it is commonly employed in clinical drug-interaction studies as a CYP2D6 inhibitor (FDA DDI guidance) and its potential effects on amine oxidase activity have not been established. Figure 5 shows the effects of high and low concentrations (10-fold difference) of each inhibitor to assess dose dependence; however, the high and low concentrations were not the same for the different compounds since low concentrations were chosen based on available maximum plasma concentrations or in vitro IC_{50} values. LJP-1207 had the most pronounced effect on emixustat deamination with complete inhibition at 1.0 μM. Semicarbazide had moderate effects at 10 μM, but more complete inhibition at 100 μM. Clorgyline and

deprenyl did not inhibit emixustat deamination in hUCM at the low concentration of 50 μM, but both inhibited at 500 μM. Neither clorgyline nor deprenyl inhibited at 10 and 100 μM in hAM. Quinidine did not inhibit oxidative deamination of emixustat in vitro, nor did β-aminoproprionitrile (BAPN; a LOX specific inhibitor; Mercier et al., 2009) in hAM even at concentrations as high as 500 μM.

In Vitro Drug-Drug Interaction Potential.

Emixustat as the victim. The reaction phenotyping for oxidative deamination of emixustat by VAP-1 infers its predominant role in the biotransformation to the three major metabolites observed in human plasma. Since metabolic clearance by VAP-1 is an uncommon pathway, its sensitivity to inhibition by other drugs as an underlying mechanism for drug-drug interactions (DDI) has been seldomly scrutinized. To assess the potential for emixustat exposure to increase in response to being victimized by an inhibitor of VAP-1, in vitro screening for VAP-1 inhibition was conducted following review of therapeutic agents with various functional moieties (e.g. hydrazine, guanidine, phthalazine) that have been demonstrated to inhibit VAP-1 activity. Additionally, inhibitors of MAO isoforms were included because they often have overlapping inhibition profiles with VAP-1/SSAO (Kinemuchi et al., 2004; Dunkel et al., 2008). Various potential inhibitors (15 compounds in total) were screened to assess their potential to inhibit the formation of ACU-5201 in pooled hAM at 60 μM concentration of emixustat which was less than maximal saturation but high enough to remain sensitive to inhibition in pooled hAM, pooled hP and rhVAP-1. Inhibition of benzylamine deamination was similarly screened at 80 μM. Most compounds were screened at a low (2 or 10 μM) and high (20 or 100 μM) concentration. Low concentrations were chosen based on available maximum plasma concentrations or published in vitro IC_{50} values for their targets and high concentrations were ten times the lower concentration. If a

compound exhibited > 50% inhibition at either of the screening concentrations, an IC_{50} was subsequently determined. Results are presented in Supplemental Table 1.

Guanabenz (20 μM), hydralazine (20 μM) and semicarbazide (100 μM) inhibited the formation of ACU-5201 by 69, 87 and 70%, respectively. The specific VAP-1 inhibitor, LJP-1207, also inhibited oxidative deamination of emixustat by more than 50%; its IC_{50} as determined in earlier hUCM experiments was 75 nM. When tested for inhibition of emixustat deamination in pooled hAM, IC_{50} values for guanbenz, hydralazine and isoniazid were 10.2, 7.4 and 55.4 μM, respectively. IC_{50} values for guanbenz and hydralazine were 46.9 and 6.4 μM when tested for inhibition of BA deamination in pooled hAM, and 9.46 and 26.5 μM in rhVAP-1, respectively. Anticipated results were observed as reported above for MAO-specific (clorgyline and deprenyl) and LOX-specific (BAPN) inhibitors. The CYP2D6 inhibitors, paroxetine and quinidine, also did not inhibit. Although benserazide (Boomsma et al., 1995) and caffeine (Olivieri and Tipton, 2011) are reported to be inhibitors of plasma VAP-1 and antidepressants have been observed to inhibit BA deamination, these compounds were not potent in vitro inhibitors of emixustat or BA deamination in vascular membranes.

Emixustat as a perpetrator. Inhibitory potential of emixustat as a perpetrator against VAP-1-mediated BA (80 μM) deamination activity in hUCM and hAM yielded IC_{50} values of 161 and 109 μM, respectively. During in vitro incubations of human plasma, 100 μM emixustat inhibited BA deamination by < 30%. More thorough kinetic analyses to determine the K_i value were performed in hUCM with emixustat concentrations of 100, 200 and 400 μM as shown in Figure 6 yielding a K_i value of 186 μM using a mixed inhibition model.

Since VAP-1 appears to be upregulated in several human pathologies (Pannecoeck et al., 2015), there are numerous published reports of VAP-1 inhibition as a potential anti-inflammatory therapy (Kinemuchi et al., 2004; Salter-Cid et al., 2005;

Dunkel et al., 2008). This study did not establish an in vitro system to examine the potential to chemically induce VAP-1, but observations were made regarding VAP-1 variability across the donor tissues. Greater variability in VAP-1 activity in the elderly aorta tissue compared to umbilical cords suggests that emixustat clearance may be more variable in an elderly population. Mean rates of emixustat deamination via vascular tissue (membrane-bound) and soluble (plasma) VAP-1 in elderly individuals were evaluated using two-way ANOVAs to determine if in vitro emixustat VAP-1 metabolism differences were discernable between select sub-populations of the demographic data in this small population of donors. There was no statistical significance between males (M) and females (F), nor between diabetics (d) and non-diabetics (n). However, Caucasians did have significantly higher emixustat metabolic rates than non-Caucasians in hAM ($p<0.005$, membrane-bound), but not in hP (soluble).

Clinical Pharmacokinetics. The mean plasma concentration–time profiles and noncompartmental PK parameters of emixustat and its 3 major metabolites, ACU-5116, ACU-5124 and ACU-5149, following daily emixustat doses of 2.5, 5 and 10 mg/kg for 7 days are shown in Figure 7 and Table 4, respectively. Mean plasma concentrations at each sample collection time point for all 3 metabolites were generally ten-fold higher than emixustat and the metabolite plasma concentration profiles declined in parallel with emixustat on both days 1 and 7 (Figure 7). Maximum plasma concentrations (C_{max}) of emixustat (~11 nM at 10 mg QD) and its three deaminated metabolites increased dose proportionally over the dose range and the average time to reach C_{max} (T_{max}) values ranged between 2.1 and 4.1 hours for all 4 analytes at all 3 dose levels indicating rapid metabolism with ACU-5116 having the earliest peak concentrations. Comparable to C_{max} values, AUC values for emixustat and its 3 metabolites ranged approximately 4- to 6-fold across the 18 individuals in each cohort, within each dose level, and their mean values increased in an apparent dose proportional manner on both days 1 and 7 consistent with

linear kinetics over the 2.5 to 10 mg dose range. AUC-based metabolite-to-parent ratios indicated plasma exposure to each inactive metabolite were 6- to 11-fold greater than to the pharmacologically active parent. Accumulation ratios of exposure (based on AUC) on day 7 ranged from 1.09 to 1.31 for emixustat and its 3 metabolites indicating minimal accumulation for any of the analytes as predicted since their elimination half-lifes ($t_{1/2}$) were a fraction of the dosing interval (24 hr). Mean elimination half-lifes of emixustat and its three metabolites were between 5.9 and 7.1 hr.

Discussion. In a previous human ADME study, three major deaminated metabolites of emixustat were identified in the plasma following a single 40 mg dose: ACU-5116, ACU-5124 and ACU-5149 (Fitzsimmons et al., 2018). The clinical PK results in subjects with geographic atrophy presented here confirm that these three deaminated metabolites predominate in plasma following single and multiple daily oral doses and reach maximum concentrations rapidly; demonstrating formation-rate limited elimination with similar $t_{1/2}$ to the parent (see Table 2 and Figure 7).

Inconsistent with these in vivo results, in vitro metabolism of emixustat in human hepatocytes resulted in a large fraction of emixustat (~34%) being unchanged with the oxidatively deaminated metabolites each accounting for a smaller fraction (4–9%) of the ^{14}C after 2 hours. The remaining metabolites observed in human hepatocytes were mainly cyclohexanol metabolites and a cyclohexanone metabolite of the hydroxypropylamine, yet none of these metabolites were ≥10% of the circulating plasma radioactivity. Although the secondary hydroxylated metabolites, ACU-5124 and ACU-5149, both achieve >10% of the total circulating plasma radioactivity, the primary metabolite, ACU-5116, appeared in human plasma more quickly than both the major secondary metabolites, emixustat (see Figure 7) or any of the other minor metabolites (Fitzsimmons et al., 2018). This suggests that formation of the major secondary metabolites occurs primarily via monohydroxylation of ACU-5116 by CYP isoform(s) (Figures 1 and 2).

Although in vivo formation of carboxylic acid metabolites from a primary amine is not a common xenobiotic biotransformation, one example is primaquine (PQ), whose major human plasma metabolite is the carboxylic acid, carboxyprimaquine (CPQ). Plasma levels of CPQ rapidly exceeded PQ concentrations with C_{max} of CPQ ten-fold higher than the parent. Even though 64% of the radioactivity of a single ^{14}C-PQ oral dose was recovered in the urine, less than 4% was due to PQ (Mihaly et al., 1984). In vivo

biotransformation of PQ to a carboxylic acid had similar conversion kinetics to that observed for emixustat and its primary carboxylic acid metabolite, ACU-5116. The high rates of emixustat deamination motivated an early study that collected portal vein blood from rats. High levels of ACU-5116, ACU-5124, and ACU-5149 were observed presystemically within 15 minutes of an emixustat oral dose (data on file).

In vitro investigations into the sequential metabolism of PQ determined that initial conversion of PQ to an aldehyde via MAO-A (Constantino et al., 1999; Pybus et al., 2012) was followed by further oxidation to CPQ by aldehyde dehydrogenase (Frischer et al., 1991). This in vitro sequential metabolism of PQ is similar to the conversion of emixustat to ACU-5116 where the initial aldol product of VAP-1 (see Figure 1) is converted to the carboxylic acid only when NAD^+ is added (Figure 2A). A similar pattern was described for tresperimus wherein aldehyde metabolites were predominantly observed following its incubation in plasma in vitro, while acid metabolites were also observed in plasma collected from humans and rats dosed with tresperimus (Claud et al., 2001). Because high levels of emixustat's acid metabolites were observed in the portal circulation of rats (as noted above), gastric mucosal and small intestinal mucosal homogenate human tissue preparations were tested alongside the rhMAO enzymes. The stability of [^{14}C]emixustat in these in vitro systems drove the decision to seek a different extra-hepatic model for emixustat oxidative deamination.

The present work indicates the biotransformation of emixustat is predominantly driven by the copper-containing amine oxidase, VAP-1. Vascular adhesion protein-1 was found to be identical in gene sequence and oxidative deamination function to SSAO (Smith et al., 1998), a member of AOC gene family that are ubiquitous across nature and distinct from FAD cofactor-containing monoamine and polyamine oxidases (Salmi and Jalkanen, 1992). As a homodimeric 180 – 200 kDa ectoenzyme with a topaquinone cofactor (Holt et al., 1998), VAP-1 is found mainly on plasma membranes of

endothelium, adipose, and smooth muscle of mammals (Barrand and Callingham, 1985, Precious et al., 1988, Wibo et al., 1980). Currently, amlodipine is the only marketed drug with oxidative deamination metabolism by a copper-containing amine oxidase (Stopher et al., 1998), yet this is a relatively minor metabolic clearance pathway. Vascular adhesion protein-1 was also established as the major metabolic clearance enzyme of the unmarketed immunosuppressive compound tresperimus (Claud et al., 2001; Claud et al., 2002).

Low to no yields of carboxylic acid metabolites in hepatocytes, liver microsomes, liver mitochondria, recombinant CYP and MAO enzymes was congruent with constitutive VAP-1 expression in sinusoidal endothelium within the liver (Lalor et al., 2002). The data presented here expands on the utility of endothelial membrane preparations for investigating VAP-1 oxidative deamination metabolism of xenobiotics that Claud et al (2002) first introduced. Similar enzyme kinetics for the oxidative deamination of emixustat to ACU-5201 were observed in hUCM, hAM and rhVAP-1 (see Table 1). The oxidative deamination activities in these sources of VAP-1 were also confirmed using BA as a marker substrate in an assay where the aldehyde product, BAL, was measured directly. The affinity of BA for VAP-1 in rhVAP-1, hUCM, hAM and hP were very similar to the previously reported values (Claud et al., 2002) and its rates of deamination were highly correlated with both the oxidative deamination of emixustat and the VAP-1 levels measured by ELISA in individual human tissue sources of VAP-1 (Figure 4 and Table 3). The variability of in vitro oxidative deamination in elderly hAM (8.8- to 17-fold) is comparable to the in vivo variability of emixustat plasma AUCs in AMD patients within each dose cohort (4- to 6-fold). This suggests that clinical variability in emixustat exposure is explained in part by interindividual variability in the expression of VAP-1 and reinforces the use of these membranes as an in vitro model for assessing the potential impact of inhibitors of VAP-1 on emixustat metabolic clearance.

DMD Fast Forward. Published on February 20, 2019 as DOI: 10.1124/dmd.118.085811
This article has not been copyedited and formatted. The final version may differ from this version.

In several mammalian species, including humans, VAP-1 has been found both on vascular cell membranes and in a soluble form in plasma, with both forms determined to be the same enzyme from protein sequencing and enzymology characterization (Smith et al., 1998). Soluble VAP-1 in human plasma may originate from proteolytic cleavage of the membrane-spanning N-terminal domains of membrane-bound homodimers, resulting in a circulating enzyme that retains deamination activity (Salmi and Jalkanen, 1992) or from circulating inflammatory endothelial cells that detach from sites of injury (Holmén et al., 2005). VAP-1 deamination in human plasma and tissues has been compared to other mammals yielding extreme variation in V_{max} values (10,000-fold), with less variation in K_M. Plasma BA deamination in humans has been reported to be comparatively low, with BA deamination in human tissues being higher than in tissues from rat and pig (Boomsma et al., 2000). Markedly higher BA deamination in human vascular membranes than in plasma are consistent with the findings in the current study. In addition, we previously reported that ACU-5201 was detected after 1 hr incubation in human plasma (Fitzsimmons et al., 2018) with 85 - 96% of [^{14}C]emixustat remaining after 1 hr in human plasma and blood. Collectively this suggests that the membrane-bound form of VAP-1 has a larger contribution to the rapid in vivo clearance of emixustat than the soluble plasma form.

Initially selective chemical inhibition was used in reaction phenotyping to confirm that ACU-5201 formation was inhibited by known inhibitors of VAP-1, but not those selective for MAO-A, MAO-B, or LOX (see Figure 5). Although inhibition of VAP-1 has been investigated extensively as an anti-inflammatory therapy over the last few decades (Kinemuchi et al., 2004; Salter-Cid et al., 2005; Dunkel et al., 2008), clinical drug interactions have yet to be observed since few drugs are eliminated by this pathway. In the absence of established clinical observations, an in vitro screening approach was undertaken for emixustat oxidative deamination. Therapeutic agents were surveyed in the

literature and screened in pooled sources of human VAP-1 to investigate the potential for inhibitory DDIs. Inhibitors and each substrate (emixustat or BA) were co-incubated prior to adding the appropriately diluted human VAP-1 sources to start the reactions. The sensitivity of the two substrates to inhibition differed by as much as 5-fold in IC_{50} values for guanabenz in hAM. A similar difference was seen for hydralazine against BA deamination in hAM relative to rhVAP-1. The homodimeric structure of VAP-1 may contribute to these differences since both cooperativity and half-site reactivity have been observed for VAP-1 (Klema and Wilmot, 2012). Additionally, formation of imine Schiff bases with primary amine substrates in the active site of VAP-1 competes with the hydrazine inhibitors as the analogous hydrazone adducts. Given the greater intrinsic hydrolytic stability of the hydrazones, time-dependent processes that were not accounted for in the coincubation design may also contribute to the differential sensitivity.

Hydralazine is a hydrazine-containing drug that was a relatively potent inhibitor of emixustat and BA deamination in pooled hAM with IC_{50} values of 7.4 and 6.4 μM, respectively. At this time the ratio of the plasma levels of VAP-1 inhibitors relative to their in vitro inhibition parameters has yet to be explored as quantitatively meaningful in assessing the likelihood of a clinically relevant drug interaction. The potential for hydralazine to have an impact on emixustat plasma exposures via VAP-1 inhibition remains valuable in identifying potential extrinsic factors that may impact therapeutic response to emixustat. Summation of the in vitro inhibition results presented here suggests that VAP-1 is relatively less sensitive to semicarbazide inhibition.

In summary, the data presented here shows that VAP-1 is predominantly responsible for emixustat oxidative deamination in human vascular membranes (hUCM and hAM) and human plasma (hP) with much higher rates in the membranes. Chemical inhibition and recombinant human enzyme strategies were effective in establishing the

role of VAP-1 in emixustat metabolism and offers a simple path for drug discovery candidates comprising primary amine to carboxylic acid biotransformations. The three major metabolites found in plasma are formed rapidly and eliminated in a formation-rate limited fashion and can be formed sequentially in vitro with additional assay components for ALDH and CYP. The rates of VAP-1 marker substrate activity and emixustat deamination were highly variable in a population of 20 elderly individuals, yet they were highly correlated with each other and VAP-1 levels measured by ELISA. Variability observed in the in vitro systems tested were similar to that observed in a clinical PK study. Most potential co-medications tested did not inhibit emixustat oxidative deamination in vitro with the exception of the vasodilators hydralazine and guanabenz. Lastly, clinically relevant inhibiton of VAP-1 by emixustat seems unlikely since its plasma concentrations are over ten thousand-fold less than the calculated K_i.

Acknowledgements

The authors thank Susan Henry, PhD (Acucela, VAP-1 ELISA); Vladimir Kuksa, PhD (Acucela, synthetic standard preparation and characterization); Lou Anne McKown (Acucela, synthetic inhibitor preparation and in vivo rat inhibitor PK analysis); Lauren Benoit (Skills Alliance, VAP-1 marker substrate assay and emixustat deamination assay); Yan Wang (Skills Alliance, VAP-1 ELISA and marker substrate assay); Galen Hall (Brown University, emixustat sequential metabolism); and Michael Fitzsimmons, PhD (Covance, plasma stability, rat portal vein ADME, MAO and hLM assays); and Inger Darling, PhD (Cognigen, PK analysis).

Authorship Contributions

Participated in research design: Podoll, Eyre, Reid.

Conducted experiments: Reid, Podoll.

Performed data analysis: Podoll, Reid.

Wrote or contributed to writing of manuscript: Reid, Podoll, Eyre.

References

Awh CC (2016) An oral drug for treatment of AMD? *Retina Today* July/August: 83-84.

Barrand MA, and Callingham BA. (1985) The interaction of hydralazine with a semicarbazide-sensitive amine oxidase in brown adipose tissue of the rat. Its use as a radioactive ligand for the enzyme. *Biochem J* **232**:415-423.

Bavik C, Henry SH, Zhang Y, Mitts K, McGinn T, Budzynski E, Pashko A, Lieu KL, Zhong S, Blumberg B, Kuksa V, Orme M, Scott I, Fawzi A, and Kubota R. (2015) Visual cycle modulation as an approach toward preservation of retinal integrity. *PLoS One* **10(5)**:e0124940. doi: 10.1371/journal.pone.0124940.

Boomsma F, van den Meiracker A, ManintVeld A, and Schalekamp M. (1995) Contrasting effects of peripheral decarboxylase inhibitors on plasma activity of aromatic-L-amino acid decarboxylase and semicarbazide-sensitive amine oxidase in Parkinson's disease. *Life Sci* **57**:1753-1759.

Boomsma F, van Dijk J, Bhaggoe UM, Bouhuizen AM, van den Meiracker AH. (2000) Variation in semicarbazide-sensitive amine oxidase activity in plasma and tissues of mammals. *Comp Biochem Physiol C Toxicol Pharmacol* **126**:69-78.

Claud P, Padovani P, Guichard J-P, Artur Y, and Laine R. (2001) Involvement of semicarbazide-sensitive amine oxidase in tresperimus metabolism in human and in rat. *Drug Metab Dispos* **29**:735-741.

Claud P, Artur Y, and Laine R. (2002) In vitro metabolism of tresperimus by human vascular semicarbazide-sensitive amine oxidase. *Drug Metab Dispos* **30**:747-755.

Constantino L, Paixão P, Moreira R, Portela MJ, Do Rosario VE, and Iley J. (1999) Metabolism of primaquine by liver homogenate fractions. Evidence for monoamine oxidase

and cytochrome P450 involvement in the oxidative deamination of primaquine to carboxyprimaquine. *Exp Toxicol Pathol* **51**:299-303.

Drug Interaction Studies — Study Design, Data Analysis, Implications for Dosing, and Labeling Recommendations, USFDA Guidance for Industry (2012)

Dunkel P, Gelain A, Barlocco D, Haider N, Gyires K, Sperlágh B, Magyar K, Maccioni E, Fadda A, and Mátyus P. (2008) Semicarbazide-sensitive amine oxidase/vascular adhesion protein 1: recent developments concerning substrates and inhibitors of a promising therapeutic target. *Curr Med Chem* **15**:1827-1839.

Fitzsimmons ME, Sun G, Kuksa V, and Reid MJ (2018) Disposition, profiling and identification of emixustat and its metabolites in humans. *Xenobiotica* **48**:592-604.

Frischer H, Mellovitz RL, Ahmad T, and Nora MV. (1991) The conversion of primaquine into primaquine-aldehyde, primaquine-alcohol, and carboxyprimaquine, a major plasma metabolite. *J Lab Clin Med* **117**:468-76.

Garpenstrand H, Ekblom J, Bäcklund LB, Oreland L, and Rosenqvist U. (1999) Elevated plasma semicarbazide-sensitive amine oxidase (SSAO) activity in Type 2 diabetes mellitus complicated by retinopathy. *Diabetic Med* **16**:514-521.

Gower NJD, Barry RJ, Edmunds MR, Titcomb LC, and Denniston AK. (2016) Drug discovery in ophthalmology: past success, present challenges, and future opportunities. *BMC Ophthalmol* **16**:11 doi 10.1186/s12886-016-0188-2.

Guideline on the Investigation of Drug Interactions, EMA Committee for Human Medicinal Products (2012)

Heuts DP, Gummadova JO, Pang J, Rigby SE, and Scrutton NS. (2011) Reaction of vascular adhesion protein-1 (VAP-1) with primary amines: mechanistic insights from isotope effects and quantitative structure-activity relationships. *J Biol Chem* **286**:29584-29593

Holmén C, Elsheikh E, Stenvinkel P, Qureshi AR, Pettersson E, Jalkanen S, Sumitran-Holgersson S. (2005) Circulating inflammatory endothelial cells contribute to endothelial progenitor cell dysfunction in patients with vasculitis and kidney involvement. *J Am Soc Nephrol* **16**:3110-3120.

Holt A, Sharman DF, Baker GB, and Palcic MM. (1997) A continuous spectrophotometric assay for monoamine oxidase and related enzymes in tissue homogenates. *Anal Biochem* **244**:384–392

Holt A, Alton G, Scaman CH, Loppnow GR, Szpacenko A, Svendsen I, and Palcic MM. (1998) Identification of the quinone cofactor in mammalian semicarbazide-sensitive amine oxidase. *Biochemistry* **37**:4946-4957.

Kinemuchi H, Sugimoto H, Obata T, Satoh N, and Ueda S. (2004) Selective inhibitors of membrane-bound semicarbazide-sensitive amine oxidase (SSAO) activity in mammalian tissues. *Neurotox* **25**:325-335.

Klema VJ and Wilmot CM. (2012) The role of protein crystallography in defining the mechanisms of biogenesis and catalysis in copper amine oxidase. *Int J Mol Sci* **13**:5375-5405

Kubota R, Boman NL, David R, Mallikaarjun S, Patil S, and Birch D. (2012). Safety and effect on rod function of ACU-4429, a novel small-molecule visual cycle modulator. *Retina* **32**:183-188.

Kubota R, Al-Fayoumi S, Mallikaarjun S, Patil S, Bavik C, and Chandler JW. (2014) Phase 1, dose-ranging study of emixustat hydrochloride (ACU-4429), a novel visual cycle modulator, in healthy volunteers. *Retina* **34**:603-609.

Kurkijärvi R, Yegutkin GG, Gunson BK, Jalkanen S, Salmi M, and Adams DH. (2000) Circulating soluble vascular adhesion protein 1 accounts for the increased serum monoamine oxidase activity in chronic liver disease. *Gastroenterology* **119**:1096-1103.

Lalor PF, Edwards S, McNab G, Salmi M, Jalkanen S and Adams DH. (2002) Vascular adhesion protein-1 mediates adhesion and transmigration of lymphocytes on human hepatic endothelial cells. *J Immunol* **169**:983-992.

Lizcano JM, Tipton KF, and Unzeta M. (1998) Purification and characterization of membrane-bound semicarbazide-sensitive amine oxidase (SSAO) from bovine lung. *Biochem J* **331**:69–78.

Marchitti SA, Brocker C, Stagos D, and and Vasiliou V. (2008) Non-P450 aldehyde oxidizing enzymes: the aldehyde dehydrogenase superfamily. *Expert Opin Drug Metab Toxicol* **4**:697-720.

Mercier N, El Hadri K, Osborne-Pellegrin M, Nehme J, Perret, C. Labat C, Regnault V, Lamaziere JM, Challande P, Lacolley P, and Feve B. (2009) Comparison of the effects of semicarbazide and β-aminopropionitrile on the arterial extracellular matrix in the Brown Norway rat *Toxicol Appl Pharmacol* **239**:258–267.

Mihaly GW, Ward SA, Edwards G, Orme ML, and Breckenridge AM. (1984) Pharmacokinetics of primaquine in man: identification of the carboxylic acid derivative as a major plasma metabolite. *Br J Clin Pharmacol* **17**:441-446.

Olivieri A and Tipton K. (2011) Inhibition of bovine plasma semicarbazide-sensitive amine oxidase by caffeine. *J Biochem Mol Tox* **25**:26-27.

Pannecoeck R, Serruys D, Benmeridja L, Delanghe JR, van Geel N, Speeckaert R, and Speeckaert MM. (2015) Vascular adhesion protein-1: Role in human pathology and application as a biomarker. *Crit Rev Clin Lab Sci* **52**:284-300.

Podoll T, Al-Fayoumi S, Eyre R, Austin, E, Prescott E, Sun G, Orme M, and Kubota R. (2013) Comparative nonclinical ocular tissue distribution of the visual cycle modulator (VCM) emixustat in rats, beagle dogs and cynomolgus monkeys. *The Toxicologist: Supplement to Toxicol Sci* **132**; 107.

Podoll T, Geisler L, Parys MV, Hanson G, and Reid MJ. (2018) Validation and reproducibility of an LC-MS/MS method for emixustat and its three deaminated metabolites in human plasma. *Bioanalysis* **10:**1803-1817.

Precious E, Gunn CE, and Lyles GA. (1988) Deamination of methylamine by semicarbazide-sensitive amine oxidase in human umbilical artery and rat aorta. *Biochem Pharmacol* **37**:707-713.

Pybus BS, Sousa JC, Jin X, Ferguson JA, Christian RE, Barnhart R, Vuong C, Sciotti RJ, Reichard GA, Kozar MP, Walker LA, Ohrt C, and Melendez V. (2012) CYP450 phenotyping and accurate mass identification of metabolites of the 8-aminoquinoline, anti-malarial drug primaquine. *Malar J* 11:259.

Salmi M, and Jalkanen S. (1992) A 90 kilodalton endothelial molecule mediating lymphocyte binding in humans. *Science* **257**:1407-1409.

Salmi M, Kalimo K, and Jalkanen S. (1993) Induction and function of vascular adhesion protein-1 at sites of inflammation. *J Exper Med* **178**:2255-2260.

Salter-Cid LM, Wang E, O'Rourke AM, Miller A, Gao H, Huang L, Garcia A, and Linnik MD. (2005) Anti-inflammatory effects of inhibiting the amine oxidase activity of semicarbazide-sensitive amine oxidase. *J Pharmacol Exp Ther* **315**:553-562.

Schwelberger HG. (2007) The origin of mammalian plasma amine oxidases. *J Neural Transm* **114**: 757-762.

Smith DJ, Salmi M, Bono P, Hellman J, Leu T, and Jalkanen S. (1998) Cloning of vascular adhesion protein 1 reveals a novel multifunctional adhesion molecule. *J Exper Med* **188**:17-27.

Smith PK, Krohn RI, Hermanson GT, Mallia AK, Gartner FH, Provenzano MD, Fujimoto EK, Goeke NM, Olson BJ, and Klenk DC. (1985). Measurement of protein using bicinchoninic acid. *Anal Biochem* **150**:76-85.

Stopher DA, Beresford AP, and Macrae PV. (1988) The metabolism and pharmacokinetics of amlodipine in humans and animals. *J Cardivasc Pharmacol* **12**:S55-S59.

van Dijk J, Boomsma F, Alberts G, Man in 't Veld AJ, and Schalekamp MA. (1995) Determination of semicarbazide-sensitive amine oxidase activity in human plasma by high-performance liquid chromatography with fluorometric detection. *J Chromatogr B* **663**:43-50.

Wibo M, Duong AT, and Godfraind T. (1980) Subcellular location of semicarbazide-sensitive amine oxidase in rat aorta. *Eur J Biochem* **112**:87-94.

Footnotes

This work was supported by Acucela Inc., and has not been previously presented.

Reprint requests should be sent to Michael J Reid, PhD, Clinical Pharmacologist, 818 Stewart Street, Suite 1110, Seattle, WA 98101 or mjr33_33@yahoo.com.

Legends for Figures

Figure 1. Oxidative Deamination Scheme of Emixustat to Its Major Metabolites. The scheme above the solid bar depicts the products formed in vitro; those below the bar represent pathways leading to the major circulating metabolites observed in vivo.

Figure 2. Sequential Metabolism of Emixustat In Vitro. A) Formation of the primary deaminated metabolite ACU-5116 in hUCM with and without NAD^+. Solid black bars represent amount of ACU-5201 (aldehyde) and checkered bars are amount of ACU-5116 (carboxylic acid). B) Formation of the secondary deaminated cyclohexanol metabolite ACU-5124 from ACU-4861 (cyclohexanol hydroxypropylamine) in hUCM with NAD^+ (top) and from ACU-5116 in hLM with NADPH (bottom). Solid black bars represent amount without cofactors and hatched bars represent amount formed with cofactors.

Figure 3. Substrate saturation curves of emixustat oxidative deamination in rhVAP-1 (green diamonds), hUCM (black triangles), hAM (blue circles) and hP (red squares).

Figure 4. Correlation of emixustat oxidative deamination with A) VAP-1 marker activity and B) protein levels in 20 individually–derived sources of hAM. Blue circles with bidirectional error bars (n=3 for activity and n=2 for ELISA) represent individual hAM values, solid blue line represents linear regression and black dots represent 95% CI.

Figure 5. Selective chemical inhibition of emixustat oxidative deamination in A) pooled hUCM and B) pooled hAM. Solid and striped bars represent low and high inhibitor concentrations, respectively, with error bars showing standard deviation of triplicate assays. Semicarbazide (green) concentrations were 10 and 100 μM in both hUCM and hAM, LJP-1207 (maroon) concentrations were 0.1 and 1.0 μM in both hUCM and hAM, β-aminoproprionitrile (βAPN LOX inhibitor; purple) concentrations were 50 and 500 μM in hAM only (B), clorgyline (black; MAO-A inhibitor) and deprenyl (blue; MAO-B

inhibitor) concentrations were 50 and 500 μM in hUCM and 10 and 100 μM in hAM and quinidine (olive) concentrations were 1 and 10 μM in both hUCM and hAM.

Figure 6. Inhibition Kinetics of Emixustat on Benzylamine Deamination in hUCM. A) Lineweaver-Burke (LB) plot with inverse BA concentrations and inverse activity rates as the X- and Y-axes, respectively. Red circles, green triangles, blue diamonds and black squares represent co-incubated emixustat concentrations of 0, 100, 200 and 400 μM, respectively. B) Plot of the LB slopes vs emixustat concentrations to determine K_i.

Figure 7. Clinical Pharmacokinetics of Emixustat and its Three Major Deaminated Metabolites A) following single 10 mg/kg oral dose and B) following daily 10 mg/kg dose on day 7 in 18 individuals with geographic atrophy. Plasma concentrations of emixustat (green diamonds), ACU-5116 (blue triangles), ACU-5124 (red squares) and ACU-5149 (black circles).

Tables

Table 1. Michaelis-Menten Kinetic Parameters for the Oxidative Deamination of Emixustat in Human Sources of VAP-1

Test System	K_M (μM)	V_{max} (pmol/min/mg protein)
rhVAP-1	13.3	2550
hUCM*	14.7 ± 1.70	309 ± 176
hAM*	15.6 ± 7.18	67.6 ± 7.98
hP	434	33.4

rhVAP-1 = recombinant human vascular adhesion protein-1, hUCM = human umbilical cord membranes, hAM = elderly human aorta membranes, hP = elderly human plasma

*Mean ± standard deviation of n = 3 different occasions, each in triplicate

DMD Fast Forward. Published on February 20, 2019 as DOI: 10.1124/dmd.118.085811
This article has not been copyedited and formatted. The final version may differ from this version.

Table 2. Michaelis-Menten Kinetic Parameters for the Oxidative Deamination of Benzylamine in Human Sources of VAP-1

Test System	K_M (μM)	V_{max} (nmol/min/mg protein)
rhVAP-1*	56.6 ± 32.7	1040 ± 506
hUCM	80.0	3.09
hAM*	78.9 ± 33.8	65.6 ± 4.64
hP[#]	75.2 ± 4.56	0.467 ± 0.024 (17.6 nmol/ml/hr)

rhVAP-1 = recombinant human vascular adhesion protein-1, hUCM = human umbilical cord membranes, hAM = elderly human aorta membranes, hP = elderly human plasma

*Mean ± standard deviation of n = 4 different occasions, each in triplicate; [#]Mean ± standard deviation of n = 3 different occasions, two in duplicate and one in triplicate

DMD Fast Forward. Published on February 20, 2019 as DOI: 10.1124/dmd.118.085811
This article has not been copyedited and formatted. The final version may differ from this version.

Table 3. Correlations of In Vitro Emixustat Oxidative Deamination Metabolism, Benzylamine Deamination and VAP-1 Levels

Correlation	Spearman		Pearson	
	r	2 tailed P	r	2 tailed P
hUCM Emixustat Deamination vs hUCM BA Deamination	0.705	<0.001	0.736	0.0018
hUCM Emixustat Deamination vs hUCM VAP-1 Levels	0.827	<0.001	0.886	<0.0001
hUCM BA Deamination vs hUCM VAP-1 Levels	0.639	<0.005	0.627	<0.005
hAM Emixustat Deamination vs hAM BA Deamination	0.794	<0.00001	0.823	<0.00001
hAM Emixustat Deamination vs hAM VAP-1 Levels	0.789	<0.00001	0.732	0.0002
hAM BA Deamination vs hAM VAP-1 Levels	0.543	0.013	0.568	0.009
hP Emixustat Deamination vs hP BA Deamination	0.922	<0.00001	0.821	0.0002
hP Emixustat Deamination vs hP VAP-1 Levels	0.874	<0.00001	0.764	0.0009
hP BA Deamination vs hP VAP-1 Levels	0.911	<0.00001	0.913	<0.00001
hAM Emixustat Deamination vs hP Emixustat Deamination	0.582	0.025	0.629	0.012
hAM Emixustat Deamination vs hP BA Deamination	0.444	0.069	0.531	0.023
hAM Emixustat Deamination vs hP VAP-1	0.486	0.041	0.477	0.045

hUCM = human umbilical cord membranes, hAM = elderly human aorta membranes, hP = elderly human plasma, BA = benzylamine, VAP-1 = vascular adhesion protein-1.

Table 4A. Mean Pharmacokinetic Parameters on Day 1 for Emixustat and Its Major Metabolites (ACU-5116, ACU-5124, and ACU-5149) in Subjects with Geographic Atrophy

Study Day	Emixustat Dose	Analyte	C_{max} ± SD [N] (ng/ml)	T_{max} ± SD [N] (h)	$t_{1/2}$ ± SD [N] (h)	AUC_{0-24} ± SD [N] (ng·h/ml)	$AUC_{0-\infty}$ ± SD [N] (ng·h/ml)
1	2.5 mg QD	Emixustat	0.637 ± 0.279 [17]	4.31 ± 1.83 [17]	5.84 ± 1.83 [16]	6.42 ± 3.39 [15]	7.15 ± 3.82 [12]
		ACU-5116	5.96 ± 2.28 [17]	2.59 ± 0.895 [17]	5.38 ± 1.96 [17]	46.1 ± 16.1 [10]	50.0 ± 21.8 [8]
		ACU-5124	7.29 ± 3.89 [17]	4.14 ± 0.956 [17]	5.72 ± 1.84 [16]	76.8 ± 42.2 [9]	80.3 ± 52.7 [8]
		ACU-5149	5.68 ± 3.02 [17	3.72 ± 0.966 [17]	5.44 ± 1.76 [16]	53.1 41.6 [9]	59.0 ± 49.3 [8]
	5.0 mg QD	Emixustat	1.61 ± 0.832 [18]	3.47 ± 1.91 [18]	6.35 ± 1.05 [17]	14.0 ± 6.15 [18]	15.0 ± 6.96 [17]
		ACU-5116	12.0 ± 5.91 [18]	2.24 ± 1.35 [18]	5.78 ± 2.66 [18]	83.4 ± 34.9 [17]	94.2 ± 44.7 [17]
		ACU-5124	13.6 ± 6.79 [18]	3.61 ± 1.10 [18]	5.57 ± 1.08 [18]	129 ± 72.8 [18]	143 ± 79.6 [17]
		ACU-5149	11.0 ± 6.18 [18]	3.42 ± 1.27 [18]	5.41 ± 1.72 [18]	101 ±70.9 [18]	110 ±79.9 [17]
	10.0 mg QD	Emixustat	2.79 ± 1.18 [18]	3.14 ± 1.49 [18]	6.78 ± 1.40 [18]	27.4 ± 12.5 [18]	30.8 ± 15.3 [18]
		ACU-5116	23.4 ± 9.04 [18]	2.66 ± 1.08 [18]	6.60 ± 2.18 [18]	168 ± 61.7 [18]	188 ± 70.6 [16]
		ACU-5124	25.3 ± 9.84 [18]	4.04 ± 1.14 [18]	6.29 ± 1.36 [18	263 ± 122 [18]	288 ± 133 [18]
		ACU-5149	21.1 ± 10.9 [18]	3.87 ± 1.25 [18]	6.12 ± 1.42 [18]	204 ± 117 [18]	223 ± 128 [18]

Table 4B. Mean Pharmacokinetic Parameters on Day 7 for Emixustat and Its Major Metabolites (ACU-5116, ACU-5124, and ACU-5149) in Subjects with Geographic Atrophy

Study Day	Emixustat Dose	Analyte	C_{max} ± SD [N] (ng/ml)	T_{max} ± SD [N] (h)	$t_{1/2}$ ± SD [N] (h)	AUC_{0-t} ± SD [N] (ng·h/ml)	R_{ac} ± SD [N]
7	2.5 mg QD	Emixustat	0.739 ± 0.372 [17]	3.92 ± 1.57 [17]	6.98 ± 1.73 [16]	7.33 ± 2.40 [14]	1.20 ± 0.152 [12]
		ACU-5116	7.34 ± 3.4 [17]	2.15 ±0.949 [17]	6.00 ± 3.26 [17]	40.8 ± 21.7 [17]	1.17 ± 0.237 [8]
		ACU-5124	7.41 ± 3.47 [17]	4.00 ± 1.50 [17]	5.89 ± 2.46 [15]	62.1 ± 44.6 [17]	1.09 ± 0.137 [6]
		ACU-5149	5.93 ± 3.77 [17]	3.35 ± 1.32 [17]	5.94 ± 2.09 [15]	49.2 ± 43.5 [17]	1.27 ± 0.392 [5]
	5.0 mg QD	Emixustat	1.69 ± 0.745 [18]	3.81 ± 1.41 [18]	7.04 ± 1.23 [18]	14.5 ± 7.55 [18]	1.19 ± 0.225 [18]
		ACU-5116	14.23 ± 6.23 [18]	2.17 ± 2.15 [18]	6.78 ± 2.85 [18]	91.4 ± 45.2 [18]	1.31 ± 0.337 [16]
		ACU-5124	16.1 ± 8.96 [18]	3.97 ± 1.46 [18]	6.95 ± 1.82 [17]	159 ± 91.0 [18]	1.24 ± 0.169 [18]
		ACU-5149	12.6 ± 6.85 [18]	3.39 ± 1.64 [18]	6.36 ± 2.01 [17]	116 ± 83.0 [18]	1.23± 0.298 [17]
	10.0 mg QD	Emixustat	3.48 ± 1.81 [18]	3.09 ± 1.32 [18]	7.05 ± 2.83 [18]	32.4 ± 17.7 [18]	1.17 ± 0.277 [18]
		ACU-5116	29.6 ± 13.o [18]	2.32 ± 1.58 [18]	6.90 ± 2.90 [17]	209 ± 100 [18]	1.27 ± 0.315 [18]
		ACU-5124	32.2 ± 16.6 [18]	4.03 ± 1.04 [18]	6.70 ± 1.64 [17]	332 ± 189 [18]	1.29 ± 0.176 [17]
		ACU-5149	23.5 ±12.8 [18]	3.75 ± 1.72 [18]	6.25 ± 1.72 [17]	239 ± 146 [18]	1.17 ± 0.230 [18]

AUC_{0-24} = area under the plasma concentration-time curve from time 0 to 24 hours; $AUC_{0-\infty}$ = area under the plasma concentration-time curve from time 0 to infinity; AUC_{0-t} = area under the plasma concentration-time curve from time 0 to the last measurable plasma concentration; AUC_{tau} = area under the plasma concentration-time curve over a 24-hour dosing interval at steady state; C_{max} = maximum observed plasma concentration; N = number of subjects; QD = once daily; R_{ac} = accumulation ratio (calculated based upon $AUC_{0-\infty}$ for emixustat and AUC_{0-24} for metabolites); SD = standard deviation; $t_{1/2}$ = terminal half-life; T_{max} = time to reach C_{max}

DMD Fast Forward. Published on February 20, 2019 as DOI: 10.1124/dmd.118.085811
This article has not been copyedited and formatted. The final version may differ from this version.

Figure 1

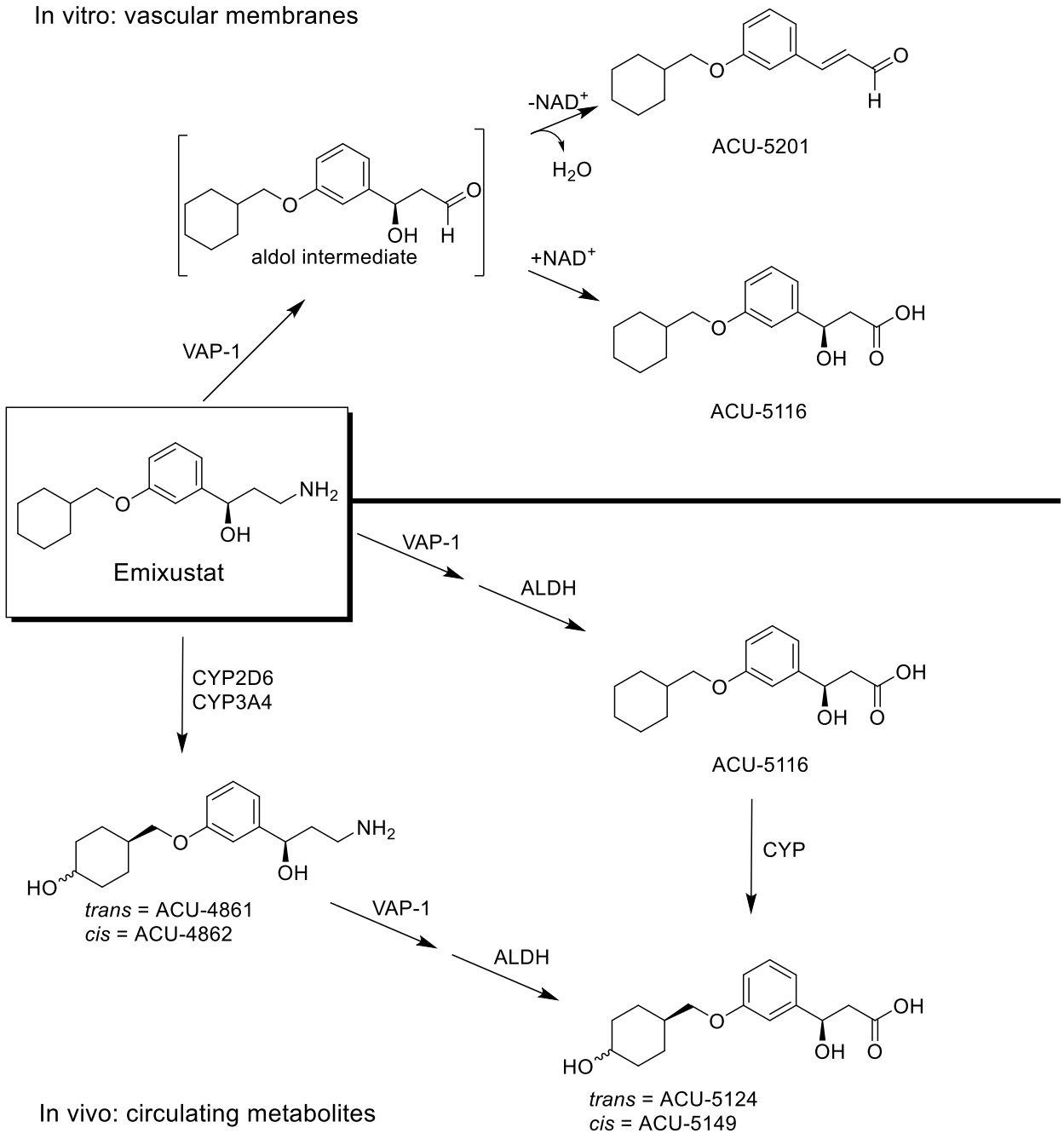

DMD Fast Forward. Published on February 20, 2019 as DOI: 10.1124/dmd.118.085811
This article has not been copyedited and formatted. The final version may differ from this version.

Figure 2

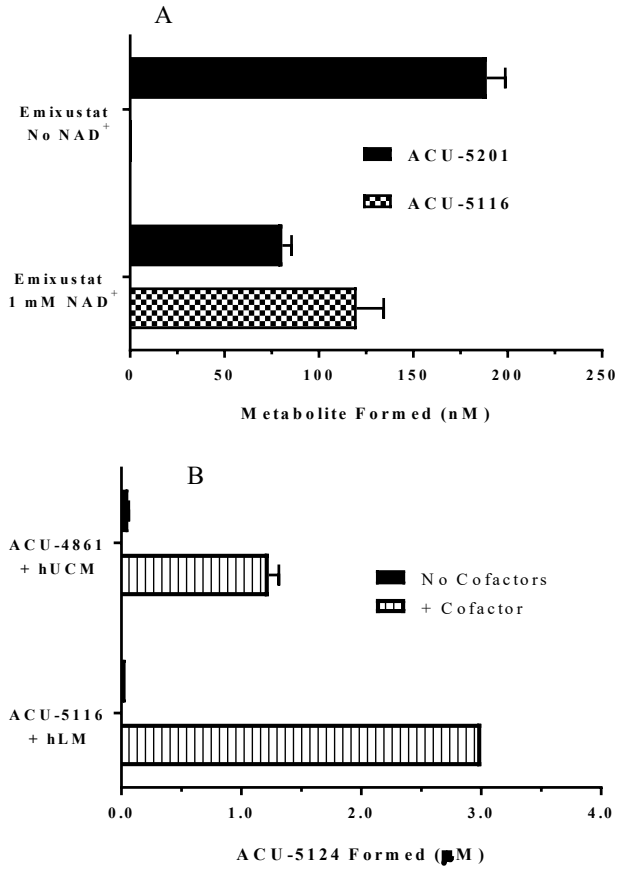

DMD Fast Forward. Published on February 20, 2019 as DOI: 10.1124/dmd.118.085811
This article has not been copyedited and formatted. The final version may differ from this version.

Figure 3

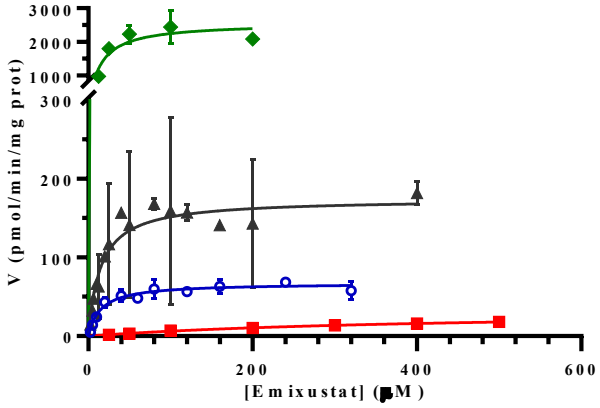

Figure 4

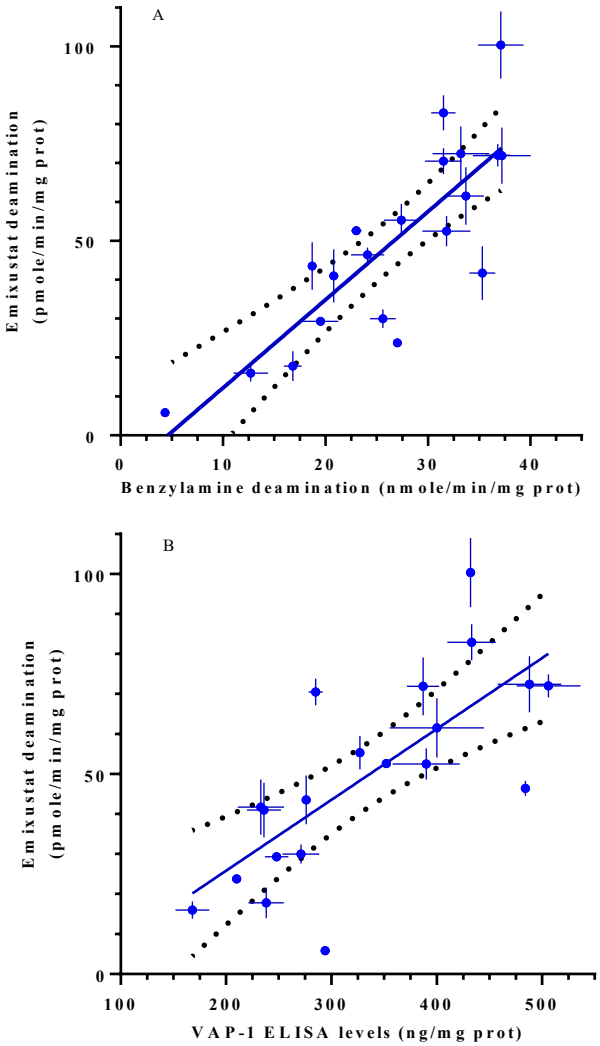

Figure 5

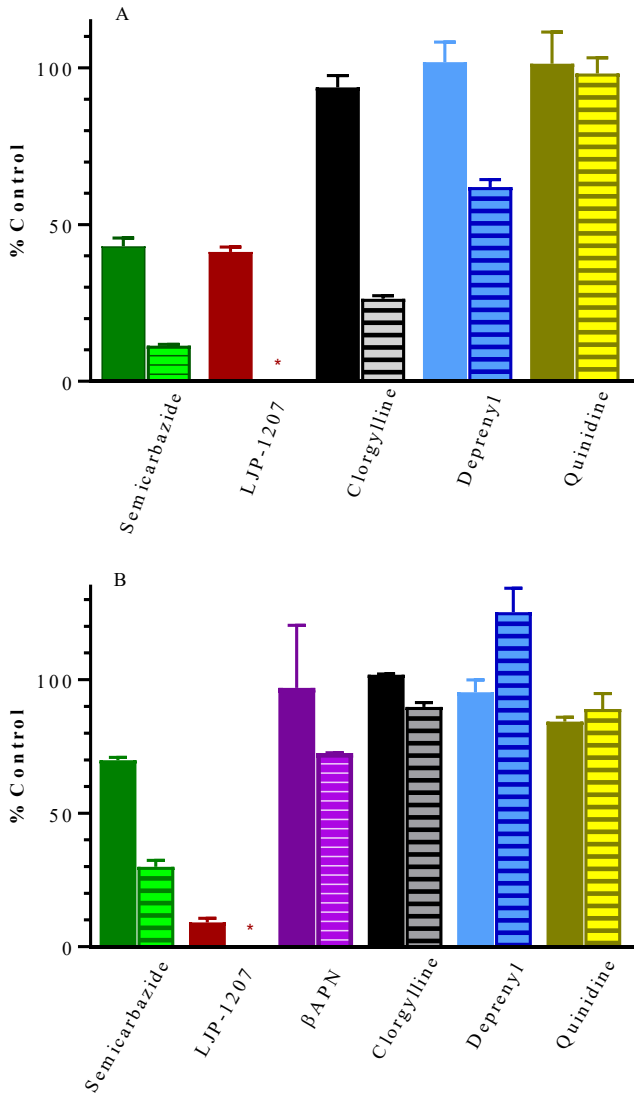

Figure 6

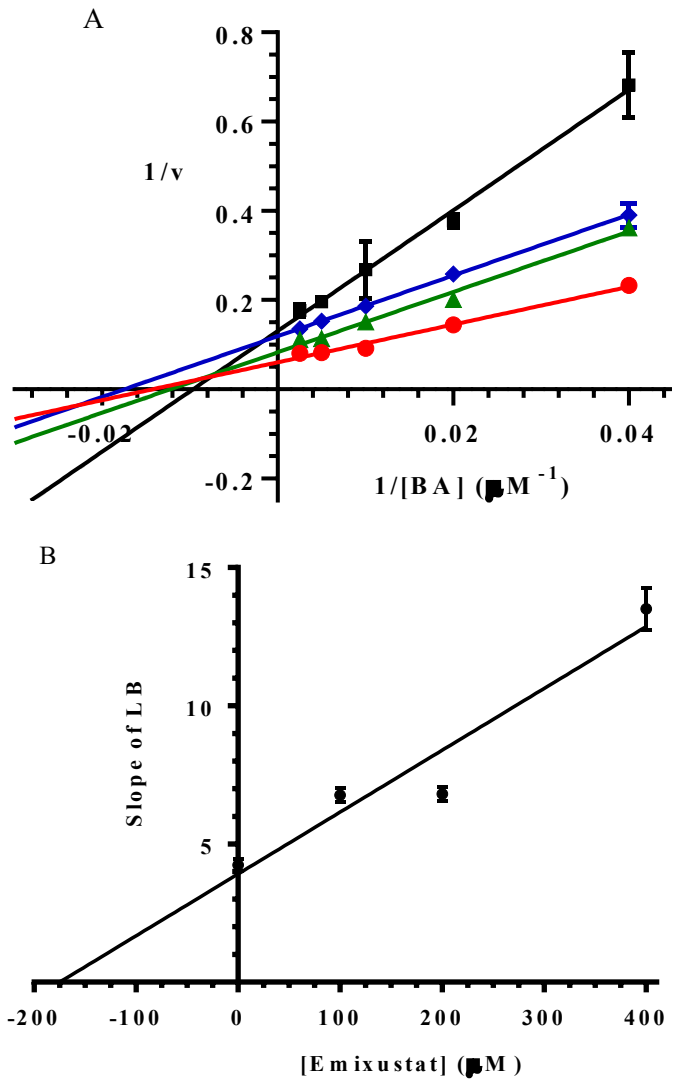

Figure 7